EURASIAN PHYSICAL TECHNICAL JOURNAL

2026, Volume 23, No. 3 (57)

https://doi.org/10.31489/2026N3/16-27

Received: 01/04/2026 Revised: 02/09/2026 Accepted: 28/09/2026 Published online: 30/09/2026

Original Research Article

Open Access under the CC BY -NC-ND 4.0 license

UDC 53.043

GROWTH AND SURFACE STRUCTURE OF FE MONOLAYERS ON Pt(110)

Toktarbaiuly O.[1,2]*, Kydyrbay N. B.[1,2], Zhazitov M. R.[1,2], Tezekbay Y. Zh.[1,2], Abduvalov A. Zh.[3], Serikov T. M.[4]

[1] Renewable Energy Laboratory, National Laboratory Astana, Nazarbayev University, Astana, Kazakhstan
[2] Institute of New Materials and Energy Technologies, Nazarbayev University, Astana, Kazakhstan
[3] School of Intelligent Systems, Astana IT University, Astana, Kazakhstan
[4] Buketov Karaganda National Research University, Karaganda, Kazakhstan
*Corresponding author: olzat.toktarbaiuly@nu.edu.kz

Abstract. *The structural evolution of Fe monolayers deposited on a Pt(110) surface was investigated under ultra-high vacuum conditions using scanning tunneling microscopy, low-energy electron diffraction, and Auger electron spectroscopy. A clean Pt(110) substrate exhibiting the characteristic (1×2) missing-row reconstruction was prepared by repeated cycles of argon ion sputtering, oxidation, and high-temperature annealing. Surface cleanliness and reconstruction were confirmed by Auger electron spectroscopy and low-energy electron diffraction, while scanning tunneling microscopy imaging revealed an anisotropic terrace–step morphology with atomic rows characteristic of the reconstructed Pt(110) surface. Fe monolayers were subsequently deposited on the clean substrate at room temperature by electron-beam evaporation. Auger electron spectroscopy measurements confirmed the presence of iron on the surface, together with minor carbon and oxygen contamination. Low-energy electron diffraction patterns recorded after Fe deposition showed a noticeable modification of the substrate diffraction features, indicating partial suppression of the original Pt(110)-(1×2) reconstruction. In addition, a sixfold diffraction feature observed at higher electron energy suggests the formation of an ordered overlayer or Moiré-type superstructure arising from the lattice mismatch between Fe and Pt(110). These results provide insight into the growth behavior and interface structure of Fe monolayers on reconstructed Pt(110), and establish a basis for future studies of iron oxide formation and redox transformations on this surface.*

Keywords: Fe growth; Pt(110); surface reconstruction; epitaxial growth.

1. Introduction

Metal-oxide interfaces play a central role in many areas of surface science, heterogeneous catalysis, corrosion, and nanostructured materials research [1–3] . Ultrathin oxide films grown on metallic substrates often exhibit structural, electronic, and catalytic properties that differ significantly from those of bulk oxides, making them valuable model systems for studying fundamental processes at the atomic scale [4–6]. In particular, well-defined oxide films supported on single-crystal metal surfaces provide an ideal platform for investigating the relationship between surface structure, chemical composition, and catalytic activity under controlled experimental conditions [7,8].

Metal surfaces, particularly noble metals, have long served as model substrates for investigations of thin film growth and surface reactions because they combine high chemical stability with well-defined

crystallographic structures [9,10]. Among noble metal substrates, platinum occupies a particularly important position due to its broad technological relevance in heterogeneous catalysis and its strong interaction with a wide range of adsorbates, metals, and oxide species. platinum surfaces are especially attractive due to their technological relevance in catalysis and their ability to support a variety of adsorbates and thin film structures [11,12]. Within the family of low-index platinum surfaces, Pt(110) has attracted special interest because of its pronounced structural anisotropy and its tendency to reconstruct under vacuum conditions. among the low-index platinum surfaces, Pt(110) has received considerable attention because of its pronounced surface reconstruction and anisotropic atomic structure [13,14].Under ultra-high vacuum (UHV) conditions, the clean Pt(110) surface reconstructs into a stable (1×2) missing-row structure [15,16]. In this reconstruction, every second atomic row along the (110) direction is removed, resulting in parallel atomic rows separated by troughs along the (001) direction [17,18]. As a result, the reconstructed surface displays a strongly anisotropic morphology composed of terraces, atomic rows, and step edges, which can act as preferential sites for adsorption, nucleation, and subsequent thin film growth [19].

A thorough examination of the structural and electronic characteristics of reconstructed Pt(110) surface has been done through different techniques such as low-energy electron diffraction (LEED), scanning tunneling microscopy (STM), and Auger electron spectroscopy (AES). [20]. Iron oxide thin films grown on metal substrates have attracted significant attention due to their complex structural behavior and important catalytic properties[20,21]. Iron oxides are widely used in applications such as environmental catalysis, oxidation reactions, and magnetic materials [22,23]. When grown as ultrathin films on metal surfaces, iron oxides can form a variety of structural phases depending on deposition conditions, oxygen exposure, and annealing temperature [24,25]. These systems therefore provide valuable model platforms for investigating oxide growth mechanisms, surface reconstructions, and redox processes at the nanoscale [1]. The Fe/Pt interface is particularly interesting because of the lattice mismatch between iron and platinum, which can lead to the formation of Moiré superstructures and other complex surface morphologies during film growth.

Previous studies have shown that the deposition of iron on noble metal substrates may result in different growth modes, including island formation, layer-by-layer growth, or mixed growth mechanisms depending on experimental conditions. Furthermore, exposure of iron films to oxygen can lead to the formation of various iron oxide phases, whose structural and electronic properties depend strongly on film thickness and substrate interactions. Understanding the oxidation and reduction behavior of iron oxide films on metal substrates is important for clarifying the stability and transformation mechanisms of these systems under reactive environments. Repeated oxidation–reduction cycles may significantly modify the morphology, composition, and surface structure of oxide films. Investigating these processes at the atomic scale is therefore essential for gaining deeper insight into the dynamics of oxide formation and reduction on metal surfaces.

In the present work, the growth and redox cycling of iron oxide films on a Pt(110) surface are investigated using a combination of scanning tunneling microscopy (STM), low-energy electron diffraction (LEED), and Auger electron spectroscopy (AES). A clean reconstructed Pt(110) surface is first prepared and characterized under ultra-high vacuum conditions. Subsequently, iron monolayers are deposited on the substrate, and their structural properties are analyzed. The system is then subjected to controlled oxidation and thermal annealing cycles to study the formation and reduction of iron oxide films. Attention is given to the evolution of surface morphology, structural ordering, and growth mechanisms during the oxidation–reduction cycling process.

2.Materials and Methods

2.1 Ultra-High Vacuum System

All experiments were carried out in an ultra-high vacuum (UHV) chamber equipped with facilities for surface preparation and analysis. The base pressure of the system was maintained at approximately 6.4^{-10} Torr during the experiments. The chamber was equipped with low-energy electron diffraction (LEED), Auger electron spectroscopy (AES), and scanning tunneling microscopy (STM) for structural and chemical characterization of the surface.

2.2 Sample Preparation

The experiments were performed using a single-crystal Pt(110) sample with a diameter of 10 mm, corresponding to a geometric surface area of approximately 78.5 mm². Prior to measurements, the surface was cleaned using repeated cycles of argon ion sputtering, oxidation, and thermal annealing. Sputtering was carried

out using an Ar^+ ion beam for approximately 20 minutes with a beam current of about 2 μA and an argon pressure of approximately 10 Pa.

Following sputtering, the sample was exposed to oxygen at a pressure of about 10 Pa for approximately 2 hours to remove residual carbon contamination from the surface. After the oxidation step, the sample was heated to approximately 480 °C and subsequently annealed at temperatures up to 1000 K. This procedure allowed carbon and oxygen contaminants to react and desorb from the surface, resulting in a clean Pt(110) surface. The cleanliness and structural ordering of the surface were verified by AES and LEED measurements. A well-defined (1×2) reconstruction characteristic of the Pt(110) missing-row structure was observed after the cleaning procedure.

2.3 Surface Characterization

Auger electron spectroscopy (AES) was used to determine the elemental composition of the surface and to monitor the presence of carbon, oxygen, and iron during the experiments. Characteristic Auger peaks corresponding to carbon and oxygen were used to evaluate surface contamination during the cleaning process.

Low-energy electron diffraction (LEED) measurements were performed to investigate the surface crystallographic structure and reconstruction of the Pt(110) surface. Diffraction patterns were recorded at different electron energies to confirm the formation of the (1×2) reconstructed surface.

Surface morphology and atomic-scale structure were examined using scanning tunneling microscopy (STM). STM measurements were performed in constant-current mode under UHV conditions. Typical tunneling parameters corresponded to a tunnel barrier of 3–4 eV. STM images were acquired to investigate the terrace structure, atomic rows, and step morphology of the reconstructed Pt(110) surface.

2.4 Iron Deposition

Fe was deposited on the clean Pt (110) surface at room temperature using an electron-beam evaporator. The deposition rate and nominal film thickness were controlled using a calibrated quartz crystal thickness monitor. The deposited Fe coverage corresponded to a few monolayers (ML), with an effective thickness of approximately 0.18 nm (1.8 Å) per Fe monolayer used for estimating the nominal coverage. After deposition, the surface was characterized using AES and LEED to confirm the presence of iron and to examine the structural changes induced by the deposited Fe atoms.

2.5 Oxidation and Reduction Cycles

Following iron deposition, the Fe/Pt(110) system was subjected to controlled oxidation and thermal annealing cycles to study the formation and reduction of iron oxide monolayers. Oxidation of the surface was performed by exposing the sample to oxygen under controlled conditions. Subsequent thermal annealing was used to induce reduction processes and modify the surface structure. The structural evolution of the surface during these oxidation–reduction cycles was monitored using AES, LEED, and STM measurements. Attention was given to changes in surface morphology, diffraction patterns, and chemical composition to understand the growth behavior of iron oxide monolayers and their transformation during repeated cycling processes.

3. Results and Discussion

3.1 Structure of the Clean Pt(110) Surface

It is a well-known fact that clean Pt(110) surface reconstructs into stable structure known as (1x2) missing row type. The crystallographic properties of the surface are given below. A top view of an fcc(110) crystal is shown in Figure 1. The surface consists of closed-packed rows in the [1-10] direction, separated by large distances in the [001] direction.

Along the [001] direction of a (1x2) missing-row reconstructed fcc(110) surface the structure repeats every four distances $d=a/\sqrt{2}$ (where a=2.77A denotes the bulk nearest-neighbor distance for platinum). Note that d is the smallest distance between atomic rows along the [001] direction if the second and deeper layers are considered. the completely arranged (1x2) arrangement, the period of 4d corresponds to a phase difference value of 2π. There exists a total of four distinguishable nonequivalently sublattice structures. Using them, it is possible to create three kinds of displacements represented by: $n\pi/2$ where n is represented by 1,2 or 3. The obtained shifts can be separated into two classes. The first-class defects having phase difference of π, 3π,… [Figures 2(b) and 2(c)] do not change the average height of surface level. The other class of defects causes a

phase shift of π/2 or 3π/2 and are necessarily correlated with the surface step [Figures 2(d) and 2(e)]. In cases when the defects belong only to the first class, phase shift of π, 3π,… , the surface fully preserves its flat appearance. Depending on the defects at the surface, two completely distinct scenarios can happen: either surface becomes non-planar or remains planar.

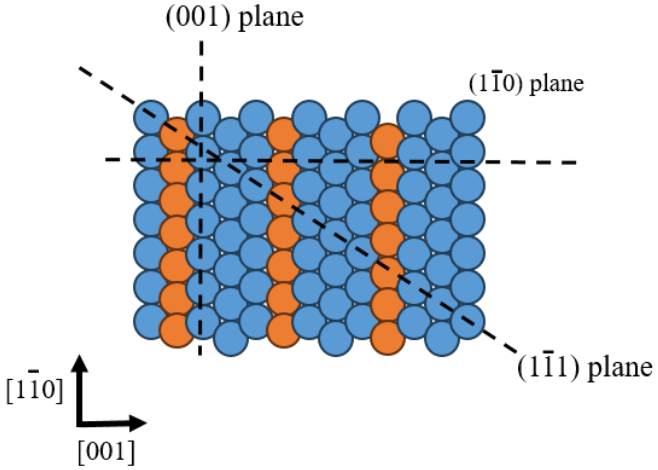


Fig. 1. Schematic top view of the fcc Pt(110) surface showing the atomic arrangement and crystallographic directions. The close-packed atomic rows run along the [110] direction, while the [001] direction corresponds to the spacing between rows. The orientations of the (001), (110), and (111) crystallographic planes relative to the surface are indicated.

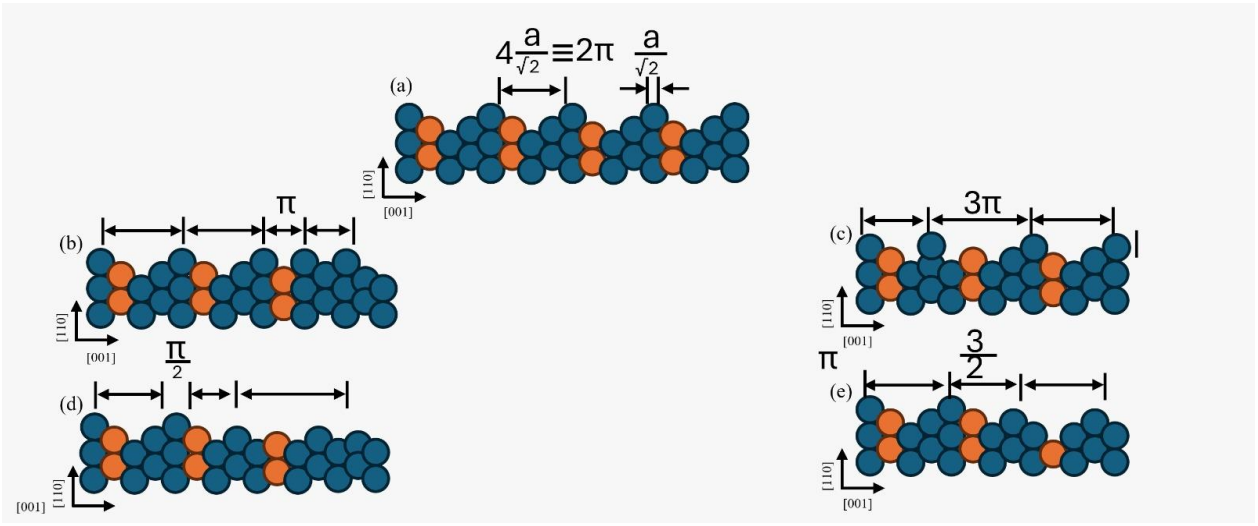


Fig. 2. Side view of the (1×2) reconstructed fcc(110) surface: (a) ideal surface with 4d periodicity along [001]; (b, c) antiphase domain walls with phase shifts of π and 3π; (d, e) surface steps with phase shifts of π/2 and 3π/2.

Figure 2 shows the (1×2) reconstructed fcc (110) surface in a side view with its surface characteristics. As illustrated in Fig. 2(a), the surface has a period of 4d along the [001]. This represents the missing-row mechanism. Here, the phase difference of 2π can be attributed to the distance between the two equivalent lattice sites on the ideal reconstructed surface and gives rise to the fundamental periodicity level in the surface system.

Two major types of surface defects are identified. The first flaw occurs in antiphase domain walls as indicated in Fig. 2(b) and Fig. 2(c). The phase difference in this case is either π or 3π. However, it must be noted that these domain boundaries do not change the height of the surface as they represent simple movements of the reconstructed rows.

The second type of defect corresponds to surface steps, as shown in Fig. 2(d) and Fig. 2(e). The phase shift for this type of defect is π/2 and 3π/2, and there is a change in the mean surface level by a single interlayer spacing. In contrast to the antiphase domain walls, the step defects involve a structural phase shift and a vertical shift of the surface. As can be seen from Fig. 2(a-e), the reconstructed Pt(110)-(1×2) surface accommodates

different types of defects by specific phase relationships, and this may play a significant role in the surface morphology and influence the Fe growth processes.

The anisotropic morphology observed for the Pt(110) surface originates primarily from the intrinsic (1×2) missing-row reconstruction of the clean surface. The reconstruction results from the removal of every second atomic row from the outermost layer along the [001] direction, producing parallel close-packed Pt rows separated by troughs. This structural arrangement gives rise to a pronounced anisotropy in the surface morphology and creates nonequivalent sites, including terraces, troughs, and step edges.

The formation of the ordered anisotropic surface proceeds through several stages. First, Ar^+ ion sputtering removes adsorbed contaminants and disrupts the outermost surface layers. Subsequent exposure to oxygen promotes the conversion and removal of residual carbon-containing species during the following thermal treatment. During high-temperature annealing, surface diffusion and atomic rearrangement become sufficiently pronounced to restore the thermodynamically stable Pt(110)-(1×2) missing-row reconstruction. Thus, the final anisotropic terrace–trough morphology is not produced directly by ion sputtering but results from the reconstruction and ordering of the Pt surface during the subsequent thermal treatment.

3.2 Structural Characterization of the Fe/Pt(110) Interface

The Pt (110) surface has been widely studied using techniques such as Low Energy Electron Diffraction (LEED), Auger Electron Spectroscopy (AES), and Scanning Tunneling Microscopy (STM), among others. In the present study, AES was used to study the Pt (110) surface. The study revealed that carbon and oxygen were present on the surface. To obtain a clean surface, Ar^+ ion bombardment coupled with an oxidation treatment was used. Subsequently, the sample was flashed, which caused the carbon-oxygen species to react, leading to desorption from the Pt (110) surface as depicted in Figure 3.

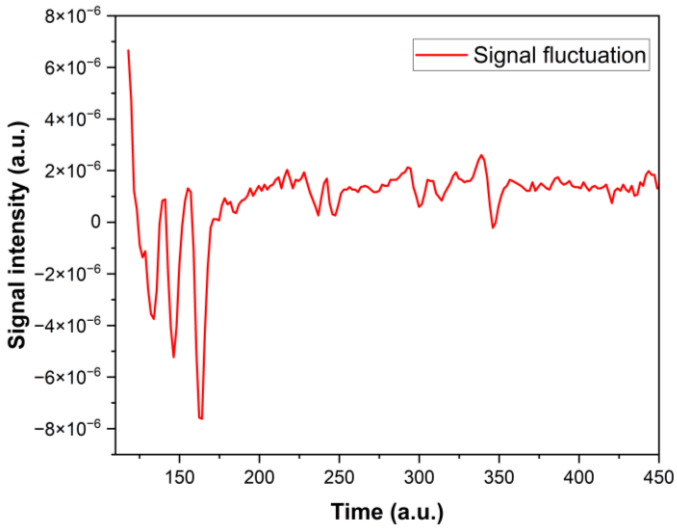


Fig. 3. Temporal evolution of the C KLL Auger signal intensity during the cleaning procedure of the Pt(110) surface. The initial transient region and subsequent quasi-stationary region are indicated.

The temporal evolution of the AES signals shown in Fig. 3–Fig. 5 provides information on the changes occurring at the Pt(110) surface during the cleaning procedure. In particular, the characteristic C KLL and O KLL Auger signals shown in Fig. 3 and Fig. 4, respectively, reflect changes in the surface concentrations of carbon- and oxygen-containing species during Ar^+ ion sputtering, oxidation, and subsequent thermal treatment. The initial transient response corresponds to the stage in which the surface composition and experimental conditions are changing. With continued cleaning and thermal treatment, the intensities of the signals associated with surface contaminants decrease and approach a quasi-stationary level. The stabilized response observed in Fig. 5 indicates that the surface composition and experimental conditions have reached a relatively stable state. The decrease in the C and O Auger signal intensities in Fig. 3 and Fig. 4, respectively, is interpreted as a reduction in the surface concentrations of carbon- and oxygen-containing species. However, the stabilization of the AES signal alone is not considered sufficient evidence of complete surface cleaning. The cleanliness and structural ordering of the Pt(110) surface were therefore evaluated using the combined AES, LEED, and STM results.

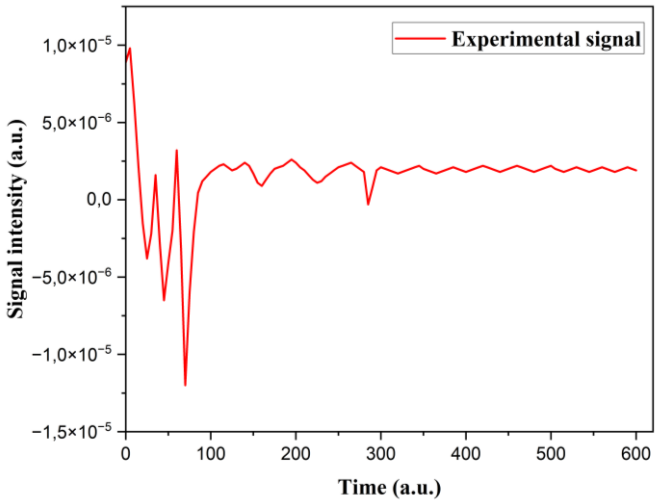


Fig. 4. Temporal evolution of the O KLL Auger signal intensity during the cleaning and annealing treatment of the Pt(110) surface. The transient and quasi-stationary regions are indicated.

The reduced C and O signals observed in Fig. 3 and Fig. 4, together with the well-defined Pt(110)-(1×2) LEED pattern in Fig. 6 and the ordered terrace–step morphology observed by STM in Fig. 7–Fig. 9, provide complementary evidence for effective removal of the major surface contaminants. The observed changes in the AES signals may result from the combined effects of Ar^+ ion bombardment, oxidation, thermal treatment, desorption of volatile surface species, and stabilization of the surface under UHV conditions. Therefore, the temporal evolution of the AES signals shown in Fig. 3–Fig. 5 is considered together with the final AES, LEED, and STM characterization when assessing the surface cleanliness and structural ordering.

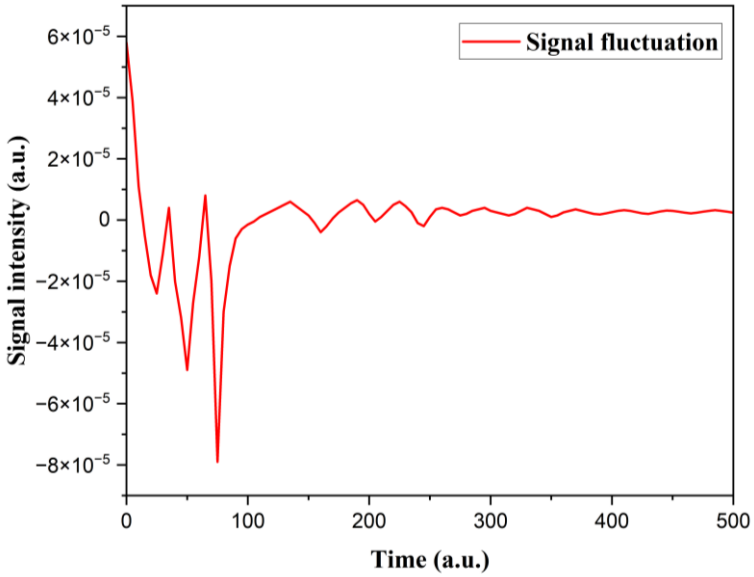


Fig. 5. Temporal evolution of the selected AES signal intensity associated with the Pt(110) surface after the cleaning procedure, showing the transition from the initial transient regime to a stable quasi-stationary state.

The structural arrangement of the Pt(110) surface and the effect of Fe deposition were investigated using low-energy electron diffraction (LEED). The LEED patterns recorded at different primary electron energies are presented in Fig. 6(a–d): (a) and (b) correspond to the clean Pt(110) surface at electron energies of 76 and 84 eV, respectively, while (c) and (d) show the corresponding patterns after Fe deposition at 82 and 92 eV. Following the annealing and flashing treatment, the clean Pt(110) surface exhibits well-defined and regularly arranged diffraction spots, confirming the formation of a well-ordered crystalline surface and indicating the successful removal of significant surface impurities. The patterns obtained at 76 and 84 eV (Fig. 6(a,b)) are qualitatively similar, demonstrating that the overall surface structure remains unchanged with variation in the

primary electron energy, although the relative intensities of the diffraction spots vary due to the energy dependence of the electron scattering process. The characteristic (1×2) features associated with the missing-row reconstruction of Pt(110) are clearly observed for the clean surface.

After Fe deposition, the characteristic (1×2) features become substantially less distinct [Fig. 6(c)], indicating that the Fe overlayer partially suppresses or modifies the long-range order of the Pt(110) missing-row reconstruction. At a primary electron energy of 92 eV (Fig. 6(d)), a distinct hexagonal diffraction pattern is observed. The appearance of six-fold symmetry indicates the formation of an ordered Fe overlayer with a periodicity different from that of the underlying Pt(110) substrate. This behavior can be associated with the development of a Moiré-type surface superstructure resulting from the lattice mismatch between the Fe overlayer and the Pt(110) surface. Thus, the LEED results demonstrate that Fe deposition modifies the reconstructed Pt(110) surface while simultaneously promoting the formation of an ordered overlayer structure.

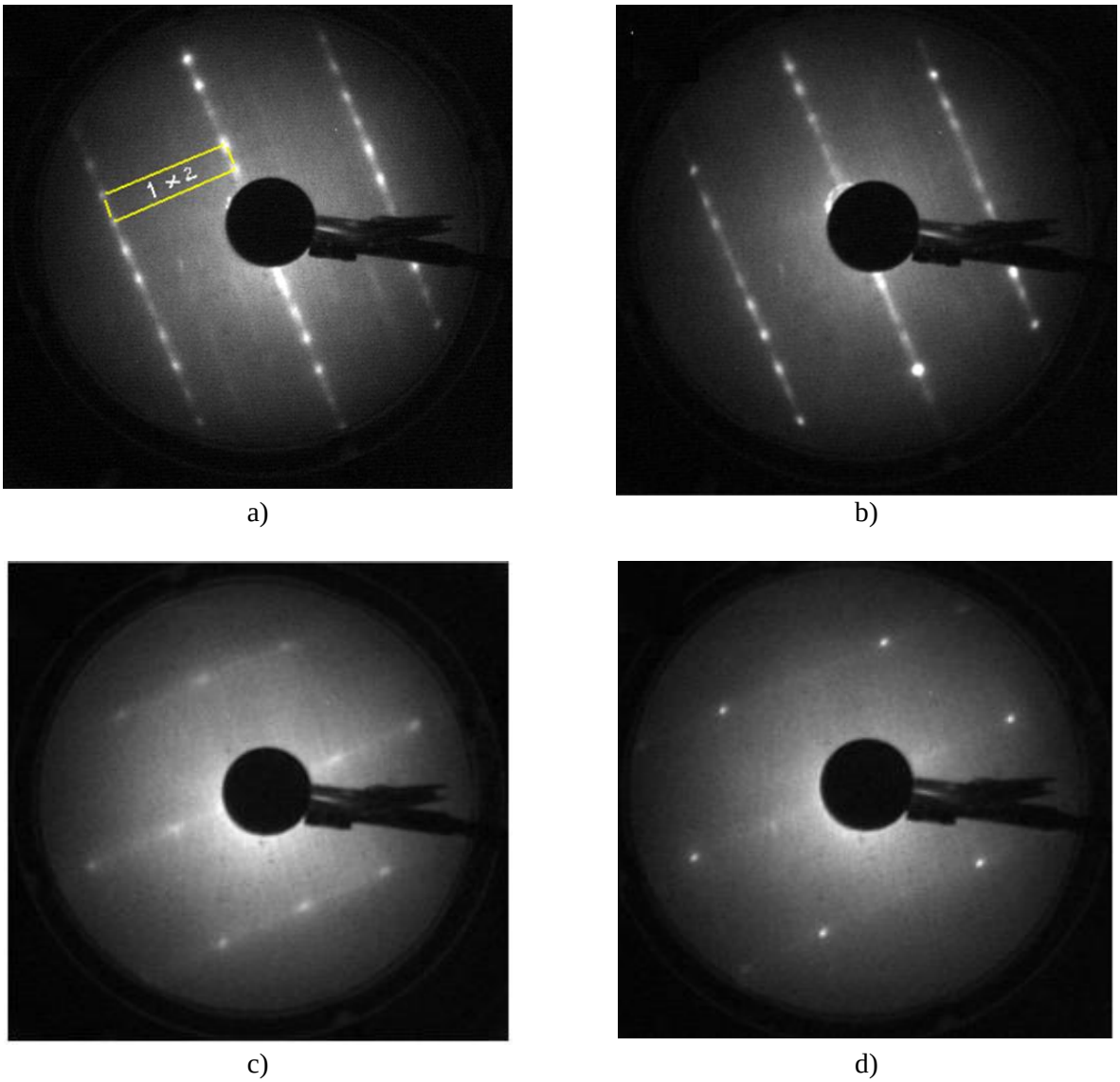
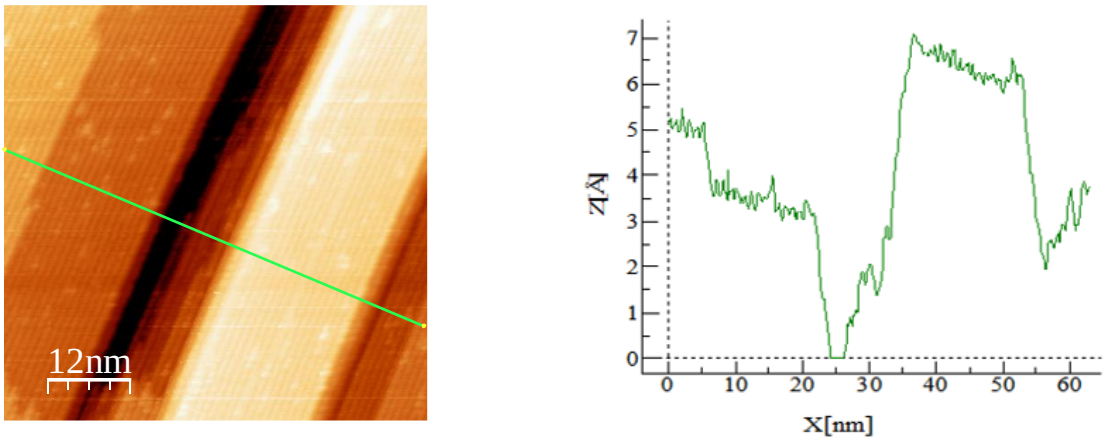


Fig. 6. LEED patterns obtained from the Pt(110) surface and Fe/Pt(110) system at different electron energies after annealing and flashing: (a) clean Pt(110), E_0 = 76 eV; (b) clean Pt(110), E_0 = 84 eV; (c) Fe/Pt(110), E_0 = 82 eV; and (d) Fe/Pt(110), E_0 = 92 eV. Fe deposition partially suppresses the missing-row reconstruction, while the hexagonal pattern in (d) indicates the formation of an ordered Fe overlayer.

Figure 7 shows a STM top view of the clean Pt(110) surface following the preparation process. As indicated in Fig. 7(a), it is evident that the surface is well ordered with features that correspond to the missing-row reconstructed Pt(110)-(1×2) surface. The presence of long-range features on the surface indicates that the surface is anisotropic in nature. This is due to the presence of atomic rows and troughs on the surface that result from the missing-row reconstruction. The STM image in Fig. 7(a) indicates that the surface is well

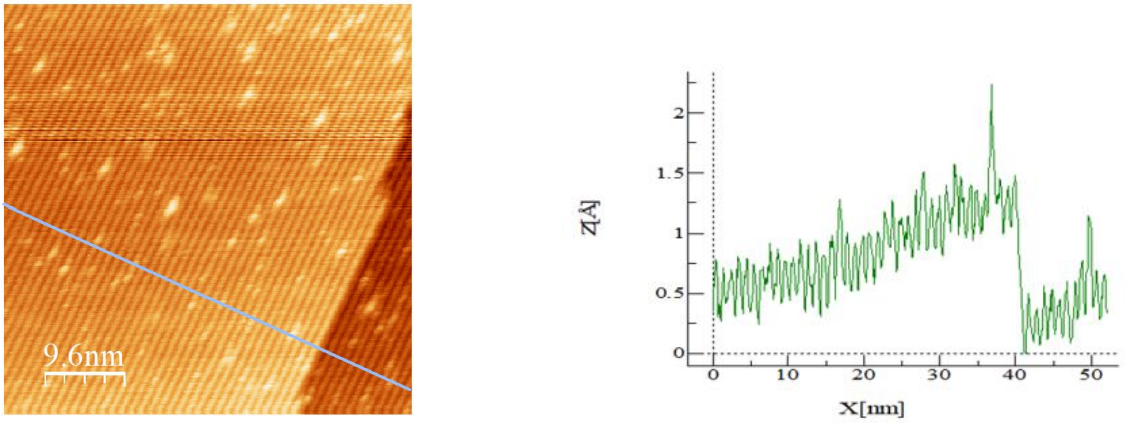
ordered at long range. However, there is also evidence of step features on the surface, which is characteristic of the missing-row reconstructed surface. The line profile in Fig. 7(b), which is indicated by the green line in Fig. 7(a), indicates that there is significant height variation on the surface. This is due to the presence of features on the surface that result in step features. The presence of the terrace-step configuration in Fig. 7(a,b) reveals that the cleaning-annealing process was effective in creating a well-structured surface, which is essential for further experimental work on Fe film depositions. The presence of terraces is also significant in Fe film growth and oxidation.



a) b)

Fig. 7. STM image of the reconstructed Pt(110) surface: (a) topography showing long-range order with step features and (b) line profile along the green line in (a), showing the terrace-step height variation. The well-structured surface confirms the effectiveness of the cleaning-annealing process.

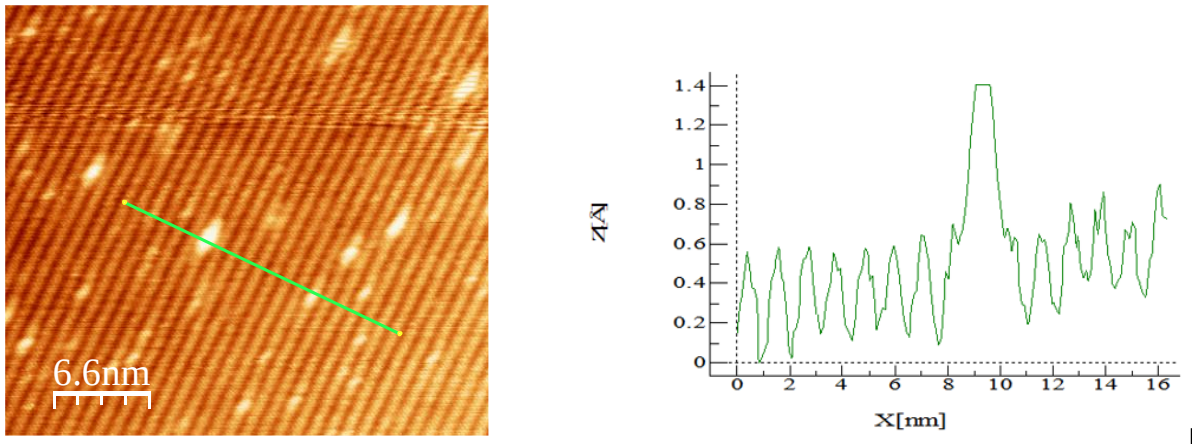
Figure 8 displays a constant current STM image of a reconstructed area of the Pt(110) surface that possesses a (1×2) reconstruction, as well as a cross-sectional profile of the reconstructed area. As seen in Fig. 8(a), the surface features a well-ordered area characterized by rows of atomic features that are characteristic of the missing row reconstructed Pt(110)-(1×2) surface. In addition to the well-ordered rows of atomic features, a well-defined step-like feature appears near the right-hand side of the reconstructed area. As seen in Fig. 8(b), the cross-sectional profile taken along the line shown in Fig. 8(a), a well-defined step appears on the surface, indicating a step-like feature on the reconstructed area of the Pt(110)-(1×2) surface. The height difference of the step appears to be around 1.4 Å, characteristic of a monoatomic step that separates terraces on the reconstructed surface. In addition, a finer corrugation, characterized by a height of approximately 0.85 Å, appears superimposed on the step profile.



a) b)

Fig.8. Constant-current STM image of (1×2) areas on the missing-row reconstructed Pt(110) surface: (a) 48 nm × 48 nm topography; (b) cross-section along the line in (a), showing a downward step.

The presence of well-ordered terraces and well-defined step edges in Fig. 8a,b implies that the Pt(110) substrate was in a very well-prepared condition after the cleaning process. The step edges are believed to be of prime importance during the process of Fe deposition because they might be used as nucleation centers for the deposited atoms. Figure 9 displays a high-resolution STM image of the reconstructed Pt(110) surface together with the corresponding cross-sectional profile taken perpendicular to the atomic rows along the [$1\bar{1}0$] direction. As shown in Fig. 9(a), the STM image clearly reveals the characteristic row structure of the reconstructed Pt(110)-(1×2) surface. In addition to the well-defined row structure, several bright features are observed, which can be attributed to surface adsorbates, such as oxygen- and carbon-containing species. The line profile presented in Fig. 9(b), taken along the direction indicated in Fig. 9(a), reveals the surface corrugation perpendicular to the atomic rows and confirms the periodicity associated with the Pt(110)-(1×2) reconstruction. The measured corrugation reaches approximately 0.8 Å, which is consistent with the characteristic row structure of the reconstructed Pt(110) surface. These observations confirm that the substrate is well ordered and suitably prepared for subsequent thin-film deposition experiments. Following preparation and characterization of the clean Pt(110) substrate, Fe thin films were deposited at room temperature using an electron-beam evaporator. The thickness of the deposited Fe films was monitored and calibrated using a quartz crystal thickness monitor. The resulting Fe/Pt(110) surfaces were subsequently characterized by Auger electron spectroscopy (AES) and low-energy electron diffraction (LEED) to evaluate their surface chemical composition and structural ordering.



a) b)

Fig.9. Large-scale STM image of the Pt(110) surface: (a) 33 nm × 29 nm topography; (b) cross-section along the line in (a), indicating the corrugation normal to the [110] rows.

The differentiated AES spectrum obtained after Fe deposition exhibits pronounced features in the 550–730 eV energy range, which are characteristic of iron Auger transitions and confirm the successful formation of an Fe overlayer on the reconstructed Pt(110) surface, as shown in Fig. 10.

In addition, weak signals attributed to carbon and oxygen are observed in Fig. 10, indicating minor residual contamination and/or partial oxidation of the deposited film. Prior to Fe deposition, AES measurements of the clean Pt(110) substrate showed almost no detectable oxygen or carbon, demonstrating that these species became more evident only after Fe deposition. This behavior, as illustrated in Fig. 10, is consistent with the higher chemical reactivity of Fe compared with Pt, which makes the deposited layer more susceptible to adsorption of residual gases under UHV conditions.

The presence of an O Auger signal after Fe deposition should not be attributed exclusively to surface contamination. Because Fe is considerably more reactive toward oxygen than Pt, the observed oxygen signal may also originate from partial oxidation of the deposited Fe layer by residual oxygen-containing species under the experimental conditions. Therefore, the O signal observed after Fe deposition is interpreted as a possible combination of residual oxygen-containing adsorbates and partial oxidation of the Fe overlayer.

The LEED observations provide a basis for further investigation of the Fe/Pt(110) interface and its evolution during oxidation and reduction. Scanning tunnelling microscopy (STM) is being employed to characterize the surface morphology of the Fe overlayer at the nanoscale, with particular emphasis on its growth mode, including the possible formation of islands and other interface-related structures. Further

experiments will focus on the oxidation of Fe/Pt(110) to produce iron oxide films, followed by characterization using Auger electron spectroscopy (AES) and LEED. Subsequent thermal annealing will be used to induce oxygen desorption and reduction of the iron oxide surface, while AES, LEED, and STM will be employed to monitor the associated structural, compositional, and morphological changes.

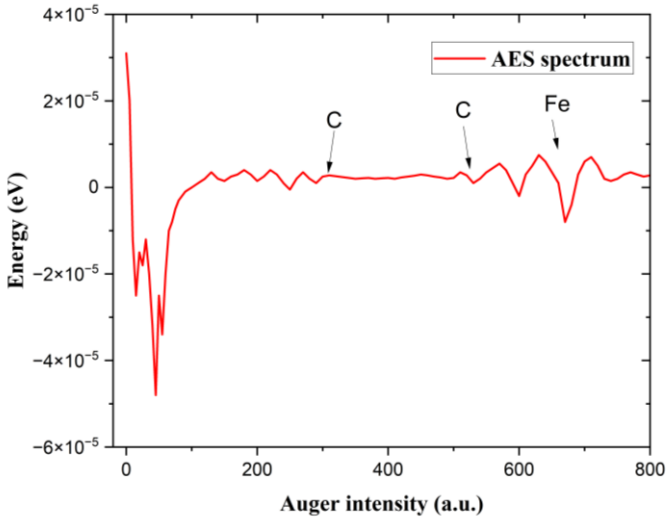


Fig. 10. Auger electron spectrum (AES) of a Fe monolayer deposited on the Pt(110) surface. The spectrum indicates the presence of iron with small contributions from carbon and oxygen, suggesting minor surface contamination.

These experiments will provide further insight into the growth and stability of iron oxide films on reconstructed Pt(110), their behavior during repeated oxidation–reduction cycles, and the morphological evolution associated with the reduction process.

4. Conclusion

In this study, the growth and structural evolution of Fe overlayers on a Pt(110) surface were investigated under ultra-high-vacuum (UHV) conditions using a combination of Auger electron spectroscopy (AES), low-energy electron diffraction (LEED), and scanning tunneling microscopy (STM). The clean Pt(110) surface, exhibiting the characteristic (1 × 2) missing-row reconstruction, was prepared through repeated cycles of Ar^+ ion sputtering, oxidation, and annealing. AES confirmed the effective removal of carbon- and oxygen-containing contaminants, while LEED demonstrated the formation of a well-ordered reconstructed surface. STM revealed the characteristic step-and-terrace morphology of Pt(110), with atomic rows oriented along the corresponding crystallographic directions. The observed step structure and surface corrugation were consistent with the expected morphology of the missing-row reconstruction.

The deposition of Fe onto the reconstructed Pt(110) surface was confirmed by AES through the appearance of Fe-related signals. Following Fe deposition, LEED revealed modifications of the characteristic Pt(110) reconstruction, together with additional diffraction features attributed to the formation of a Moiré-type superstructure. These observations demonstrate that Fe deposition significantly modifies the structural ordering of the Pt(110) surface and results in the formation of a well-defined Fe/Pt(110) interface. The structural characterization performed in the present study establishes Fe/Pt(110) as a suitable model system for investigating the subsequent formation and evolution of iron oxide on a metallic substrate.

Future experiments will focus on the controlled oxidation of the Fe overlayer under UHV conditions. The resulting iron oxide phases will be characterized using AES, LEED, and STM to determine their chemical composition, crystallographic structure, and surface morphology. Particular attention will be paid to the effects of Fe coverage, oxygen exposure, and annealing temperature on oxide formation and structural ordering. These studies will provide insight into the oxidation behavior and structural evolution of Fe/Pt(110) interfaces and contribute to a better understanding of model metal–oxide interfaces relevant to surface chemistry, catalysis, and oxidation–reduction processes.

Conflict of interest statement
The authors state that they do not have any form of conflict of interest concerning their research, whether it is financial, personal, related to authorship and so on, that might interfere with the research itself, and results mentioned in this article.

CRediT author statement
Toktarbaiuly O.: Investigation and Supervision; **Kydyrbay N.B.:** Conceptualization, Writing – original draft; **Zhazitov M.R**..: Methodology, Writing - review & editing; **Tezekbay Y.Zh**.: Investigation & Validation; **Abduvalov A.Zh.:** Data curation, Formal analysis; **Serikov T.M.:** Visualization; Review and Editing. The final manuscript has been approved, and it has been perused by all authors.

Statement on the use of Artificial Intelligence.
During the preparation of this manuscript, artificial intelligence tools were used solely for language editing and grammatical improvement.

Data Availability Statement
The data are available upon reasonable request from the authors.

Funding

The funding for this research has been provided by the Science Committee at the Ministry of Science and Higher Education (MHES) of the Republic of Kazakhstan under Grant No. AP23488359.

References

1. Somorjai, G. A., & Li, Y. (2010). *Introduction to surface chemistry and catalysis* (2nd ed.). John Wiley & Sons. https://www.wiley-vch.de/en/areas-interest/natural-sciences/introduction-to-surface-chemistry-and-catalysis-978-0-470-50823-7
2. Freund, H.-J., Kuhlenbeck, H., & Staemmler, V. (1996). Oxide surfaces. *Reports on Progress in Physics, 59*(3), 283–347. https://doi.org/10.1088/0034-4885/59/3/002
3. Campbell, C. T. (1997). Ultrathin metal films and particles on oxide surfaces: Structural, electronic and chemisorptive properties. *Surface Science Reports, 27*(1–3), 1–111. https://doi.org/10.1016/S0167-5729(96)00011-8
4. Freund, H.-J., & Pacchioni, G. (2008). Oxide ultra-thin films on metals: New materials for the design of supported metal catalysts. *Chemical Society Reviews, 37*(10), 2224–2242. https://doi.org/10.1039/B718768H
5. Diebold, U. (2003). The surface science of titanium dioxide. *Surface Science Reports, 48*(5–8), 53–229. https://doi.org/10.1016/S0167-5729(02)00100-0
6. Wintterlin, J., & Bocquet, M.-L. (2009). Graphene on metal surfaces. *Surface Science, 603*(10–12), 1841–1852. https://doi.org/10.1016/j.susc.2008.08.037
7. Vlieg, E., Robinson, I. K., & Kern, K. (1990). Relaxations in the missing-row structure of the (1×2) reconstructed surfaces of Au(110) and Pt(110). *Surface Science, 233*(3), 248–254. https://doi.org/10.1016/0039-6028(90)90636-M
8. Sowa, E. C., Van Hove, M. A., & Adams, D. L. (1988). The missing-row model for the reconstructed Pt(110)-(1×2) surface: A LEED intensity analysis showing multilayer distortions. *Surface Science, 199*(1–2), 174–182. https://doi.org/10.1016/0039-6028(88)90406-2
9. McIntyre, B. J., Salmeron, M., & Somorjai, G. A. (1993). In situ scanning tunneling microscopy study of platinum (110) in a reactor cell at high pressures and temperatures. *Journal of Vacuum Science & Technology A, 11*(4), 1964–1968. https://doi.org/10.1116/1.578531
10. Minca, M., Penner, S., Loerting, T., Menzel, A., Bertel, E., Zucca, R., & Redinger, J. (2007). Chemisorption of hydrogen on the missing-row Pt(110)-(1×2) surface. *Topics in Catalysis, 46*(1–2), 161–167. https://doi.org/10.1007/s11244-007-0326-4
11. Fery, P., Moritz, W., & Wolf, D. (1988). Structure determination of the (1×2) and (1×3) reconstructions of Pt(110) by low-energy electron diffraction. *Physical Review B, 38*(11), 7275–7284. https://doi.org/10.1103/PhysRevB.38.7275
12. Doná, E., Cordin, M., Deisl, C., Bertel, E., Franchini, C., Zucca, R., & Redinger, J. (2009). Halogen-induced corrosion of platinum. *Journal of the American Chemical Society, 131*(8), 2827–2829. https://doi.org/10.1021/ja809674n
13. Pedersen, T. M., Li, W.-X., & Hammer, B. (2006). Structure and activity of oxidized Pt(110) and α-PtO_2. *Physical Chemistry Chemical Physics, 8*(13), 1566–1574. https://doi.org/10.1039/B515166J
14. Pendry, J. B. (1974). Low-energy electron diffraction. In *Interaction of atoms and molecules with solid surfaces* (pp. 201–211). Springer. https://doi.org/10.1007/978-1-4684-8777-0_7
15. Briggs, D., & Seah, M. P. (Eds.). (1990). *Practical surface analysis, Volume 1: Auger and X-ray photoelectron spectroscopy* (2nd ed.). John Wiley & Sons. ISBN 0-471-92081-9.
16. Chen, C. J. (2021). *Introduction to scanning tunneling microscopy*. Oxford University Press. https://academic.oup.com/book/41125
17. Bode, M. (2003). Spin-polarized scanning tunnelling microscopy. *Reports on Progress in Physics, 66*(4), 523–582. https://doi.org/10.1088/0034-4885/66/4/203

18. Spiridis, N., Wilgocka-Ślęzak, D., Freindl, K., Figarska, B., Giela, T., Młyńczak, E., & Korecki, J. (2012). Growth and electronic and magnetic structure of iron oxide films on Pt(111). *Physical Review B, 85*(7), Article 075436. https://doi.org/10.1103/PhysRevB.85.075436

19. Ritter, M., Ranke, W., & Weiss, W. (1998). Growth and structure of ultrathin FeO films on Pt(111) studied by STM and LEED. *Physical Review B, 57*(11), 7240–7247. https://doi.org/10.1103/PhysRevB.57.7240

20. Lewandowski, M., Pabisiak, T., Michalak, N., Miłosz, Z., Babačić, V., Wang, Y., Korecki, J., & Kiejna, A. (2018). On the structure of ultrathin FeO films on Ag(111). *Nanomaterials, 8*(10), Article 828. https://doi.org/10.3390/nano8100828

21. Shipilin, M., Lundgren, E., Gustafson, J., Zhang, C., Bertram, F., Nicklin, C., & Merte, L. R. (2017). Fe oxides on Ag surfaces: Structure and reactivity. *Topics in Catalysis, 60*(6–8), 492–502. https://doi.org/10.1007/s11244-016-0714-8

22. Soldemo, M., Niu, Y., Zakharov, A., Lundgren, E., & Weissenrieder, J. (2015). A well-ordered surface oxide on Fe(110). *Surface Science, 639*, 13–19. https://doi.org/10.1016/j.susc.2015.04.008

23. Seidel, P., Pomp, S., Schwarz, F., & Sterrer, M. (2025). Stability and dissolution of single-crystalline iron oxide thin films in electrochemical environments. *Surface Science, 751*, Article 122621. https://doi.org/10.1016/j.susc.2024.122621

24. Venables, J. A. (1994). Atomic processes in crystal growth. *Surface Science, 299–300*, 798–817. https://doi.org/10.1016/0039-6028(94)90698-X

25. Brune, H. (1998). Microscopic view of epitaxial metal growth: Nucleation and aggregation. *Surface Science Reports, 31*(4–6), 125–229. https://doi.org/10.1016/S0167-5729(99)80001-6

AUTHORS' INFORMATION

Toktarbaiuly, Olzat. – Ph.D., National Laboratory Astana, Nazarbayev University, Astana, Kazakhstan; ORCID iD: 0000-0003-4594-3435; olzat.toktarbaiuly@nu.edu.kz

Kydyrbay, Nazerke S. – Master (Sci.), National Laboratory Astana, Nazarbayev University, Astana, Kazakhstan; ORCID iD: 0009-0002-6067-7817; nazerke.kydyrbay@nu.edu.kz

Zhazitov, Mergen R. – National Laboratory Astana, Nazarbayev University, Astana, Kazakhstan; ORCID iD: 0009-0008-3494-1067; olzat.toktarbaiuly@nu.edu.kz

Tezekbay, Yerbolat Zh. - Master (Sci.), National Laboratory Astana, Nazarbayev University, Astana, Kazakhstan, Kazakhstan; ORCID iD: 0000-0001-7479-6898; yerbolat.tezekbay@nu.edu.kz

Abduvalov, Alshyn Zh. - Ph.D., Associate Professor, School of Intelligent Systems, Astana IT University, Astana,

Kazakhstan ORCID iD: 0000-0003-4252-8674; alshyn.abduvalov@astanait.edu.kz

Serikov, Timur M. – Ph.D., Associate Professor, Buketov Karaganda National Research University Karaganda, Kazakhstan; ORCID iD: 0000-0003-4302-9674; serikov-timur@mail.ru